

# Potential and current distribution in strongly anisotropic $\text{Bi}_2\text{Sr}_2\text{CaCu}_2\text{O}_8$ single crystals at current breakdown

I. Pethes,<sup>1</sup> A. Pomar\*,<sup>2</sup> B. Sas,<sup>1</sup> G. Kriza,<sup>1</sup> K. Vad,<sup>3</sup> Á. Pallinger,<sup>1</sup> F. Portier,<sup>2</sup> and F. I. B. Williams<sup>2</sup>

<sup>1</sup>Research Institute for Solid State Physics and Optics, PO Box 49, H-1525 Budapest, Hungary

<sup>2</sup>Service de Physique de l'Etat Condensé, Commissariat à l'Energie Atomique, Saclay, F-91191 Gif-sur-Yvette, France

<sup>3</sup>Institute of Nuclear Research, PO Box 51, H-4001 Debrecen, Hungary

(Dated: November 18, 2018)

Experiments on potential differences in the low-temperature vortex solid phase of monocrystalline platelets of superconducting  $\text{Bi}_2\text{Sr}_2\text{CaCu}_2\text{O}_8$  subjected to currents driven either through an  $ab$  surface or from one such surface to another show evidence of a resistive/nonresistive front moving progressively out from the current contacts as the current increases. The depth of the resistive region has been measured by an in-depth voltage probe contact. The position of the front associated with an injection point appears to depend only on the current magnitude and not on its withdrawal point. It is argued that enhanced nonresistive superconducting anisotropy limits current penetration to depths less than the London length and results in a flat rectangular resistive region with simultaneous  $ab$  and  $c$  current breakdown which moves progressively out from the injection point with increasing current. Measurements in  $ab$  or  $c$  configurations are seen to give the same information, involving both  $ab$ -plane and  $c$ -axis conduction properties.

PACS numbers: 74.72.Hs, 74.25.Fy, 74.25.Sv

## I. INTRODUCTION

Understanding the current and the potential distributions at the onset of dissipation in a superconductor is important; at a fundamental level for interpreting the results of transport measurements in terms of the force-velocity relation for the vortices and the Josephson coupling between layers as well as on a practical level for understanding how to maximize the current carrying capacity of a wire. The family of high- $T_c$  cuprate superconductors naturally raises the question of the influence of high anisotropy on current carrying properties. How does one interpolate between the extreme anisotropic limit, where current injected into a superconducting plane has no transfer to other planes, and the isotropic case where the penetration of the current in the superconducting state is determined by the London screening length.<sup>1</sup> To give a concrete illustration of the problem, a naive interpretation of the threshold current for dissipation in a strongly anisotropic  $\text{Bi}_2\text{Sr}_2\text{CaCu}_2\text{O}_8$  (BSCCO) single crystal based on penetration limited to the London screening length or, even more naively, supposed to be uniform over the typical thickness of a few micrometers gives threshold current densities one to two orders of magnitude lower than a standard interpretation of a magnetic hysteresis loop.

Anisotropy is a central feature of the family of the high- $T_c$  cuprate superconductors which are usually modeled by discrete superconducting sheets parallel to the  $ab$  crystallographic plane weakly coupled together in the  $c$  direction by extended Josephson junctions.<sup>2</sup> The weak

coupling between planes gives rise to very high conduction anisotropy in both the normal and superconducting states. It is also responsible for the richness of the phase diagram of the vortices created when one applies a magnetic field. A convenient experimental probe for investigating these phases, particularly as regards their pinning to the host lattice disorder, is to look at the voltage response to transport current ( $VI$  characteristics) for currents which take one into the resistive regime where the vortices are dislodged. But to interpret these measurements correctly, it is important to know about the current distribution in the resistanceless regime, how it is modified as dissipation sets in and of course what the potential distribution then looks like.

It was remarked some time ago,<sup>3</sup> in connection with resistivity experiments, that if the response of the superconductor is Ohmic,  $\mathbf{E} = \rho \cdot \mathbf{J}$  (the resistivity tensor  $\rho$  is constant and independent of current and position), the problem may be treated as for the normal state where it is implicit that the phase slip giving rise to the voltage also relaxes the magnetic dephasing to allow the current to penetrate beyond the London screening depth. In this regime, at least, the high anisotropy of the (BSCCO) samples studied limited the current penetration into the depth of the sample to a small fraction of its thickness and that it would therefore be quite erroneous to deduce a critical current density on the basis of uniform penetration across the section of a short sample. Experiments to date on the current profile have been able to show a concentration of current towards the sample edges, but have been insensitive to the depth dependence<sup>4</sup> which is the aspect that interests us chiefly here.

The present paper reports an experimental investigation and a few basic reflections on this problem in the non-Ohmic, low-temperature, high magnetic-field vortex solid phase, also in monocrystalline BSCCO in a

\*Present address: Institut de Ciència de Materiales de Barcelona, CSIC, Campus de la UAB, 08193 Barcelona, Spain

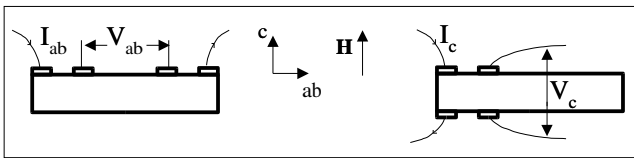


FIG. 1:  $ab$  and  $c$  contact configurations.

$c$ -directed magnetic field. The experiment consists of measuring the voltage response to short pulses of current up to and beyond dissipative breakdown. Potentials are measured at contacts placed in the usual way on the  $ab$  faces supplemented by in-depth potential contacts to have direct access to depth-dependent features. One of the important points that emerges is that the physically unrelated  $c$ -axis and  $ab$ -plane dissipative breakdowns interact to create a resistive/nonresistive front which has the effect of altering the current distribution and giving rise to a critical current which involves both  $ab$  and  $c$  characteristics. Not only does the voltage response along an  $ab$ -plane surface into which the current is injected and withdrawn (the “ $ab$  configuration” of Fig. 1) show features of the Josephson junctions between planes, but also the response to current injection and withdrawal on opposing  $ab$ -plane faces (the “ $c$  configuration” of Fig. 1) shows features of breakdown in the  $ab$  plane. One manifestation of this is that the threshold current in the  $ab$  configuration on BSCCO single crystals<sup>5</sup> shows the same temperature and preparation dependence as for the  $c$  configuration.<sup>6</sup> This brings up the question as to who measures what and does one measure what one thinks; but beyond that what do the results mean?

## II. EXPERIMENTAL TECHNIQUE

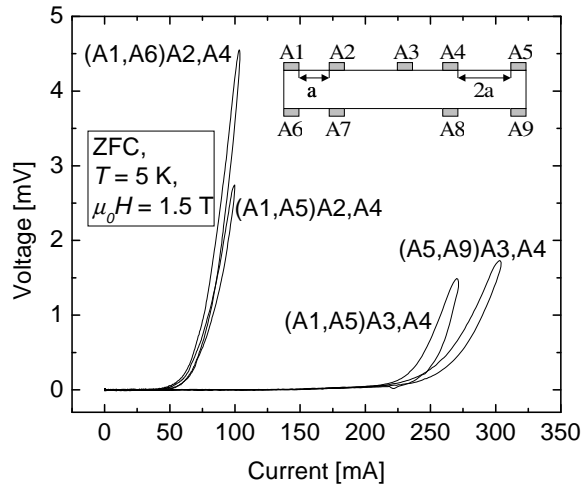
Our samples are thin monocrystalline platelets with the  $c$  axis perpendicular to the face. As all the samples studied gave qualitatively the same results for similar contact configurations, we limit ourselves here to the results on one sample of each different contact configuration. The sizes of samples  $A$ ,  $B$ , and  $C$  are about  $2 \times 0.35 \times 0.005 \text{ mm}^3$ ,  $1.1 \times 0.3 \times 0.002 \text{ mm}^3$ , and  $0.7 \times 0.5 \times 0.005 \text{ mm}^3$ . They were all fabricated by a melt cooling technique.<sup>7,8</sup> The critical temperatures were between 88 and 90 K with a transition width of about 2 K at zero field. The anisotropy coefficient  $\gamma_n \approx 500$  was estimated from normal-state resistivities with  $\rho_{ab} \approx 100 \mu\Omega \text{ cm}$  at 90 K. In the case of samples  $A$  and  $B$ , electrical contact was made by bonding 25- $\mu\text{m}$  gold wires with silver epoxy fired at 900 K. For sample  $C$  the contacts were made by depositing silver on a lithographically defined area using a lift-off technique and heat treating at 700 K for 1000 s. In all cases the contact resistance was less than  $3 \Omega$ . The sample was mounted flat against a 7-mm-diameter 0.5-mm-thick sapphire disk with silicone grease to ensure thermal homogeneity and mechanical freedom

and placed in the bore of a superconducting magnet with the field along the  $c$  direction. The sample and disk were surrounded by exchange gas and the temperature was electronically regulated. The longitudinal voltage-current ( $VI$ ) characteristics were measured by a symmetrized differential four-point technique using 25- $\mu\text{s}$  triangular pulses (12.5  $\mu\text{s}$  from zero to maximum current) of maximum amplitude in the range  $10 \text{ mA} < I_m < 350 \text{ mA}$ , usually restricted to exceed the threshold by about 30%, with repetition time 0.1 s. As reported earlier,<sup>5</sup> the observed threshold is independent of pulse duration for times up to about 250  $\mu\text{s}$ , argued there to be the time required for heat produced in the current contact to diffuse towards the voltage contact, whereas bulk heating in the superconductor was estimated not to be important. Further technical details may be found in Ref. 5.

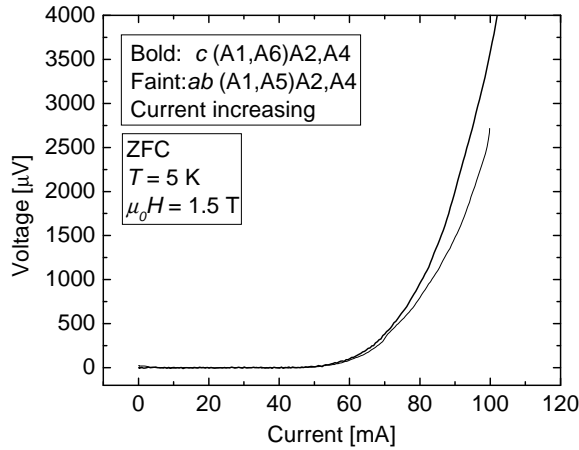
## III. EXPERIMENTAL RESULTS

We present first the results of experiments on the  $VI$  response with surface contacts in the standard  $ab$  and  $c$  configurations on the same sample using contacts common to the two configurations. The results lead rather naturally to a description in terms of resistive/nonresistive fronts moving outwards from the current contacts. Experiments are then presented for other surface contact configurations intended to check this hypothesis. These are followed by experiments with a different type of contact configuration designed to probe the depth of the sample as breakdown progresses.

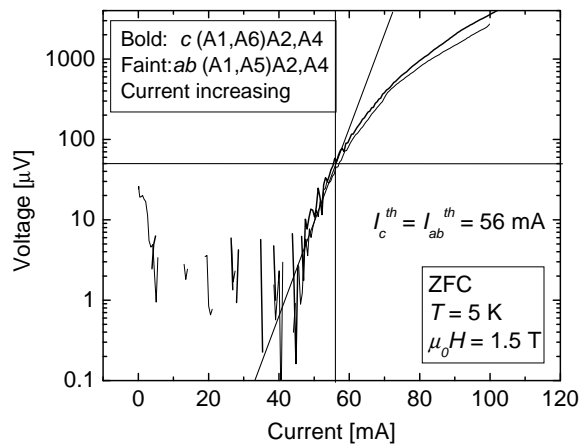
The first experiment was done on samples contacted to be able to measure in both  $ab$  and  $c$  configurations on the same sample at the same time as illustrated in Fig. 2. The “ $ab$  configuration” measurements refer to the potential drop between contacts ( $A2, A4$ ) for current injected at  $A1$  and withdrawn from  $A5$ . The “ $c$  configuration” refers to the potential measured across ( $A2, A7$ ) for current passed through ( $A1, A6$ ). Figure 3 shows the temperature dependence of the threshold current in the  $VI$  characteristic at 1.5 T in sample  $A$  for both configurations. The threshold current is defined by the break in slope criterion of Ref. 5 which gives essentially the same values as the criterion of crossover from Kim-Anderson behavior at low current to power law close to linear behavior at higher current,<sup>9</sup> illustrated in detail for the first pair of curves of Fig. 2 in the semilog plot in the same figure. The measured thresholds, as represented in Fig. 3, are seen to be independent of the configuration, whether the sample is field cooled (FC) or zero-field cooled (ZFC) prepared, despite the fact that the two preparations give different thresholds for temperatures lower than the peak in the ZFC results.<sup>5</sup> For the FC preparation, the field is applied above  $T_c$  and the sample is cooled at constant field to the lowest measuring temperature, subsequent measurements being made on increasing the temperature at the same field. For ZFC preparation, the system is cooled in zero field from above  $T_c$  to the lowest



(a)



(b)



(c)

FIG. 2:  $VI$  curves measured on sample A. The letters on the  $VI$  curves refer to the contacts used: the first pair in brackets denote the current contacts and the last two the potential contacts. The inset in (a) shows the contact configuration. Part (a) shows the response to up and down current sweeps of isocles triangular shape of total duration  $25 \mu\text{s}$ . Parts (b) and (c) show in more detail, on both linear and semilogarithmic plots, upswing response for the first two curves of part (a).

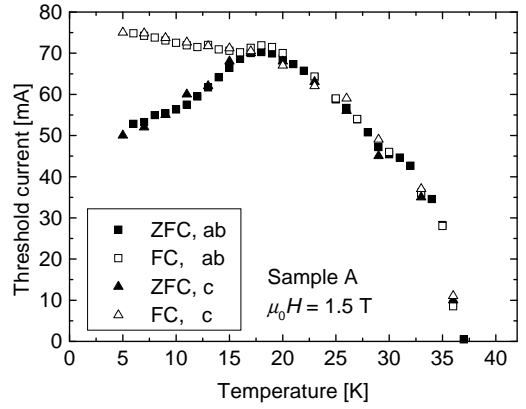


FIG. 3: Temperature dependence of the threshold current with  $ab$  and  $c$  contact configurations on the same sample.

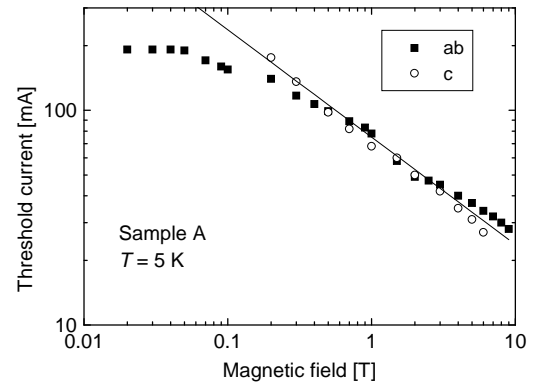


FIG. 4: Magnetic-field dependence of the threshold current with both contact configurations on the same sample. The solid line shows  $H^{-1/2}$ .

temperature before applying the field and then making measurements at sequentially higher temperatures at the same field. Figure 4 shows the magnetic-field dependence in both contact configurations for ZFC preparation at 5 K on increasing the field (FC preparation followed by field variation gives the same result, except for the initial FC prepared point<sup>9</sup>). At fields above about 0.3 T, the threshold currents for the two different configurations again show the same behavior, this time in field, varying approximately as  $H^{-1/2}$ . Not only are the temperature and field dependences of the threshold currents in the two configurations similar in form, but the values themselves coincide. Measurements along several other lines in the  $(H, T)$  plane confirm this indistinguishability of  $ab$  and  $c$  configuration thresholds as generic behavior for the low-temperature high-field domain. This fact led us to look in more detail with the following experiment.

Again referring to the inset of Fig. 2, we used three potential contacts ( $A2, A3, A4$ ) on the top layer and two ( $A7, A8$ ) on the bottom. The contact  $A2$  is half as far away from the left current contact  $A1$  as is the contact  $A4$  from the right-hand current contact  $A5$ , while  $A3$  is

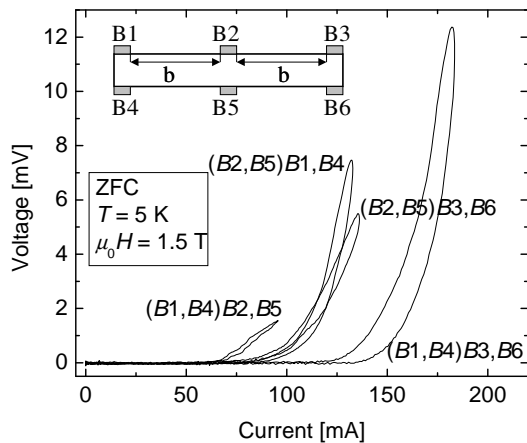


FIG. 5:  $VI$  response of sample  $B$ . The labeling convention is as before.

midway between the two current contacts. If we apply the current between contacts  $A1$  and  $A5$  ( $ab$  direction) we measure a much lower threshold current between  $A2$  and  $A4$  than between  $A3$  and  $A4$ . On the other hand, we find virtually identical  $VI$  curves on the  $ab$  potential contacts ( $A2, A4$ ) whether the current is applied in the  $c$  direction through contacts ( $A1, A6$ ) or along the  $ab$  direction ( $A1, A5$ ); similarly the  $VI$  across ( $A3, A4$ ) is nearly identical for  $ab$ -directed current through ( $A1, A5$ ) or for  $c$ -directed current through ( $A5, A9$ ).

These results suggest the idea that the sample first becomes resistive around the injection points and that this resistive region progressively invades the sample as the current is increased. This led us to experiment with the contact configuration of sample  $B$  illustrated in Fig. 5 where we drove the current through the  $c$  direction and also measured the voltage drop across that direction. On sending the current through ( $B1, B4$ ) the  $VI$  characteristic measured across ( $B2, B5$ ) shows a threshold current which is about half that measured across contacts ( $B3, B6$ ). On the other hand, if we put the current through the middle contacts ( $B2, B5$ ) we find the same threshold at either of the two end potential contacts ( $B1, B4$ ) or ( $B3, B6$ ) with a value intermediate between the previous two.

Although these experiments lend considerable support to the idea of a resistive/nonresistive front progressing along the surface, they say nothing about its profile with depth since at no point were we able, in this low-temperature high-field phase and despite micron thin samples, to drive the lower face contacts resistive with current sent along the top face. To have more direct information about the shape of the front with depth, we prepared a third sample  $C$  as in Fig. 6 with a lithographically defined terrace argon ion etched along the length of one  $ab$  face to a depth of 220 nm. The upper part of the face was also argon ion etched to avoid any difference in surface pinning between it and the terrace, the width of which was restricted to a small fraction (20%) of the

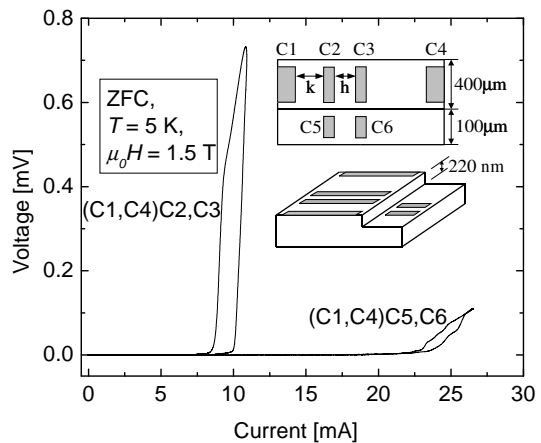


FIG. 6:  $VI$  response for sample  $C$ . The dimensions  $k$  and  $h$  are 125  $\mu\text{m}$  and 75  $\mu\text{m}$ , respectively. The potential contact dimension along the sample length is 50  $\mu\text{m}$ .

total sample width to minimize the trivial effect of current spread as the distribution attains the depth of the terrace. The contacts were accurately aligned between the two levels by a scanning electron-beam masking microscope. On a control sample with the same contact configuration but with no terrace, the  $VI$  response on contacts ( $C2, C3$ ) gave the same values of the threshold current and dynamic resistance as contacts ( $C5, C6$ ), themselves very similar to those for the top contacts of the terraced sample.

Sending an  $ab$ -directed current through contacts ( $C1, C4$ ) on the upper part of the face, we measured the potential drop across ( $C2, C3$ ) on the upper part and across ( $C5, C6$ ) on the step. The threshold current for the terrace contacts is considerably higher than for the corresponding top contacts: about 25 mA and 10 mA, respectively, much greater than the decrease of 20% in the current density to be expected from simple current spread into the wider part of the sample. We interpret the large difference to arise from the current distribution with depth.

#### IV. INTERPRETATION OF EXPERIMENTAL RESULTS

All these observations are consistent with the idea of a resistive front moving progressively outward from the current contacts as illustrated for sample  $A$  in Fig. 7. Also, and more surprisingly, it seems that the position of the front depends only on the magnitude of the current injected and seems to be independent of its ultimate destination if one is to account for the nearly identical  $VI$  response on, for example, the potential contact pair ( $A2, A4$ ) independently of whether the current is withdrawn on the same face ( $A1, A5$ ) or the opposite face ( $A1, A6$ ); similarly for the potential pair ( $A3, A4$ ) for current through ( $A1, A5$ ) or ( $A5, A9$ ). The difference

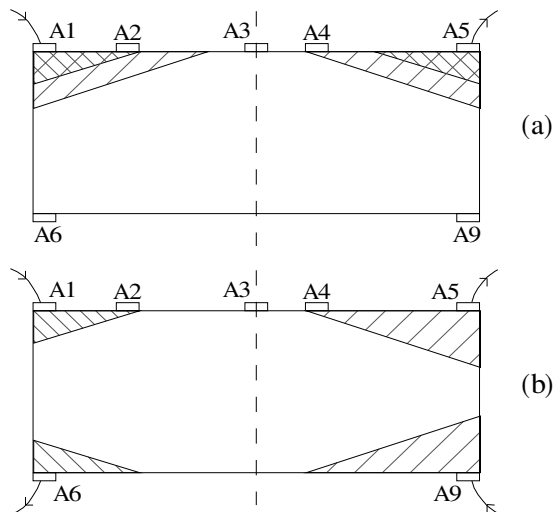


FIG. 7: Schematic illustration of a lengthwise section of sample *A* showing the propagation of resistive fronts with current directed in the (a) *ab* direction (*A1*, *A5*) and (b) *c* direction (*A1*, *A6*) or (*A5*, *A9*). The *c* axis is vertical.

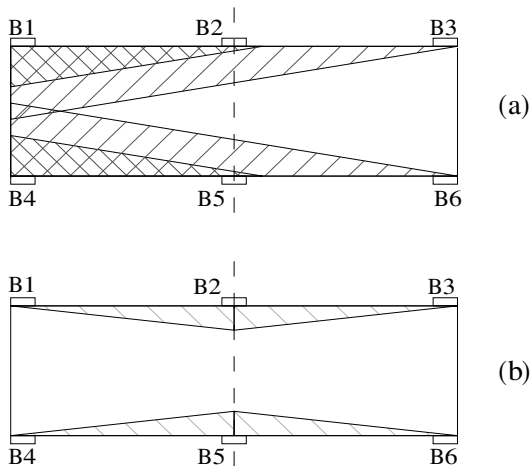


FIG. 8: Schematic illustration of the propagation of resistive fronts with a *c*-directed current in a lengthwise section of sample *B*. The current was driven through (a) (*B1*, *B4*) contacts near one end of the sample (b) (*B2*, *B5*) at the middle of the sample.

between the values of the threshold current measured on (*A2*, *A4*) and (*A3*, *A4*) contact pairs is accounted for by the distances of the potential contact from the nearest current contact (*A2* from *A1* or *A4* from *A5*). In these experiments, the fronts did not attain contact *A3* which remained at the potential of the resistanceless region. The triangular form used for the resistive region in the figure is purely schematic to show the progression of the front. Further consideration of possible forms is given below where it is argued that the form is in fact most probably rectangular.

Figure 8 represents how the resistive front is imagined

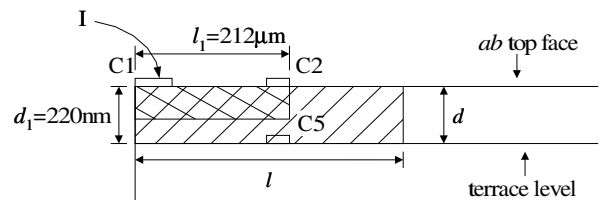


FIG. 9: Schematic illustration of a section of sample *C* with an etched terrace to investigate depth dependence of the resistive/nonresistive front which propagates from current contact *C1* to attain the top surface contact *C2* and, at higher current, the terrace contact *C5*. If the front were rectangular as illustrated and had a current-independent aspect ratio  $\ell/d$ , the dimensions would be linear in the total current and  $\ell/d = (\ell_1/d_1)(I_{d_1}^{\text{th}}/I_{\ell_1}^{\text{th}})$  provided that  $I_{d_1}^{\text{th}} \geq I_{\ell_1}^{\text{th}}$ .

to progress in the experiment with sample *B* when the current is run through the *c* direction. Here too the lower threshold current was obtained for potential pair (*B2*, *B5*) nearest the current contacts. The resistive front from current contacts (*B1*, *B4*) attains (*B2*, *B5*) before (*B3*, *B6*). When the current was run through the middle of the sample by (*B2*, *B5*) the injected current is divided between two directions with a corresponding reduction in current density so that the voltage drop appears at higher current for the same distance and gives the same response at both ends.

Figure 9 represents the front for the experiment with the terraced sample. Here the form of the front has been taken to be rectangular for the reasons outlined in the following section. As the front is defined by the line at which the current density reaches the threshold for resistive breakdown (*ab* plane and/or *c* direction) the integral of the threshold current density crossing the front is just the total current. Furthermore if the front does not change geometrical form with current amplitude its dimensions increase linearly with the current. Then, knowing the distance from the nearest current contact and the depth of the terrace, the threshold current values for the upper and step contacts give information on the depth and potentially some information on the form of the front as it attains the upper and terrace level contacts. We can expect the aspect ratio of the front to be related to the anisotropy.

## V. ELEMENTARY UNDERSTANDING

We shall assume for the present discussion that edge effects are not a dominant factor for our observations. Although we expect an integrable singularity at the edge of the sample, a large part of the middle of the sample has an essentially flat distribution with distance from the center line<sup>20</sup> and we deal in the first instance uniquely with the distribution with depth  $\hat{z}$  and along the length  $\hat{x}$  of the sample. We know that in the normal resistive state the current distribution is governed by the anisotropy of

the resistivity. By rescaling the coordinates according to the anisotropy factor  $\gamma_n = \sqrt{\rho_c/\rho_{ab}}$  the problem can be solved as a Laplace equation in the potential. The necessary coordinate rescaling is determined by the anisotropy factor  $\gamma$ :  $z \rightarrow \gamma z$ . In the normal state, it is clearly given by  $\gamma_n^2 = \rho_c/\rho_{ab} \approx (500)^2$  and would give rise to an  $ab$  current penetration depth of about  $p_{ab} \sim \ell_{ab}/\gamma_n \sim 1 \mu\text{m}$  for a distance  $\ell_{ab} = 1 \text{ mm}$  between  $ab$  current contacts.<sup>3</sup>

It is less recognized, perhaps, that the low current distribution in the nonresistive superconducting regime can be governed by the same sort of equation for the superconductor phase in similarly rescaled coordinates if the penetration depth is smaller than the London screening depth. In the nonresistive superconducting phase, the Laplacian in the potential is replaced by a Laplacian in the superconductor phase which has the same form of relationship to the superconducting current as does the potential to the current in the normal state. The anisotropy ratio in the superconducting state is given by  $\gamma_s^2 = (n_s e \hbar / m_{ab}) / s J_J$ , the ratio of the coefficients of the  $ab$  and  $c$  phase gradients in the relation between the current operator and the phase. The  $s J_J$  term is the low current expansion of the Josephson relation between successive superconducting planes separated by  $s$ , while  $n_s$  is the three-dimensional (3D) superconducting electron density and  $1/m$  the inverse mass tensor. If one were to neglect London screening,  $\gamma_s$  would govern the current penetration in the same way as does  $\gamma_n$  in the normal state.

The superconducting anisotropy is usually expressed as a mass ratio or London screening length ratio for  $c$  and  $ab$  currents  $\gamma_s^2 = m_c/m_{ab} = \lambda_c^2/\lambda_{ab}^2$  and is customarily expected to have about the same value as the extrapolated normal-state resistivity ratio. In BSCCO, however, experiments<sup>10</sup> on mesa structures have shown a Josephson critical current reduced by a factor of about 30 with respect to the usual Ambegaokar-Baratoff<sup>11</sup> relation to the high current resistance; the low current resistive slope is proportionately altered to  $V_{\text{gap}}/s J_J \approx 30 \rho_c$  and the coefficient in the Josephson relation  $J_z = J_J \sin(\varphi_n - \varphi_{n+1}) \rightarrow s J_J \partial \varphi / \partial z$  at low current is reduced by the same factor with a corresponding enhancement of the anisotropy factor [ $\varphi_n$  is the phase  $\varphi(\mathbf{r})$  of the superconductor wave function at the  $n$ th superconducting plane]. This has been attributed to the  $d$ -wave nature of the order parameter and already enhances the anisotropy factor by  $\sqrt{30}$  over the normal state. But if one also considers the effect of phase fluctuations across the Josephson junction caused by misalignment of vortices in magnetic field, another multiplicative factor  $\langle \cos \varphi_{n,n+1} \rangle^{-1/2}$  should be incorporated into  $\gamma_s$ . The factor  $\langle \cos \varphi_{n,n+1} \rangle$  has been variously estimated from Josephson plasma resonance<sup>12</sup> experiments to be between about  $10^{-3}$  and  $10^{-1}$ , extrapolating to about  $4 \times 10^{-3}$  (Refs. 13 and 14) at low temperature and  $\mu_0 H = 1.5 \text{ T}$ , which suggests a very strongly enhanced anisotropy parameter in the superconducting phase as compared with the normal state:  $3 \times 10^4 < \gamma_s < 1 \times 10^6$ . Current penetration in the super-

conducting phase is governed by a combination of London screening and anisotropy, both of which act to limit the penetration. But, even before including the effects of London screening, the anisotropy limits the penetration depth  $p_{ab} \sim \ell_{ab}/\gamma_s$  in the middle of a 1-mm-long BSCCO sample to  $2 < p_{ab} < 20 \text{ nm} \ll \lambda_{ab} \simeq 200 \text{ nm}$ . Thus in short samples of BSCCO like ours the current penetration in the superconducting phase is always dominated by anisotropy rather than by London screening.

This suggests that the effective thickness for current flow might be given approximately by  $p_{ab} \sim \ell_{ab}/\gamma_s < \lambda_{ab} \ll t$  (the real thickness), and furthermore that the current density is nonuniform along the sample, being higher closer to the contacts, causing breakdown to resistive behavior to be progressive and not to penetrate immediately throughout the bulk. Under these conditions,  $ab$  breakdown alone is not possible: if only  $ab$  breakdown were to occur, the front would have to be parallel to the  $c$  direction because no part of the interface with the nonresistive region can be parallel to the electric field produced along the  $ab$  breakdown direction. But if breakdown does not occur uniformly throughout the thickness of the sample, the front must somewhere change orientation. The electric field in the resistive portion, which must be oriented perpendicular to the interface, therefore also changes orientation and that requires  $c$  breakdown. Hence a resistive/nonresistive front within the sample which does not go straight through it along a principal direction necessarily implies simultaneous  $ab$  and  $c$  breakdown. The regions of  $ab$  and  $c$  breakdown need not be spatially coincident however, but they must be at least contiguous. The same can be argued for the case of pure  $c$  breakdown.

Another consequence of the nonuniformity of the current distribution in depth is the presence of shear forces on the vortices and the possibility of sliding between planes of (semi)ordered vortex segments.<sup>3,15</sup> This has important consequences on the locality of the  $\mathbf{E}(\mathbf{J})$  relation. If the force required to shear two adjoining planes derives from an effective Josephson coupling  $J_J \langle \cos \varphi_{n,n+1} \rangle$ , the condition for nonelastic shear (slip) is  $\partial J_{ab} / \partial z \gtrsim J_J \langle \cos \varphi_{n,n+1} \rangle a / s^2$ , where  $a$  and  $s$  are the distances between vortices in the plane and the distance between neighboring planes, respectively. Using the expression for the anisotropy penetration depth  $p_{ab} \sim \ell_{ab}/\gamma_s$  and identifying the effective Josephson coupling with the  $c$ -axis critical current density  $J_c^{\text{th}}$ , the condition for shear to occur at the onset of dissipation is  $J_{ab}^{\text{th}}/J_c^{\text{th}} \gtrsim \gamma a \ell_{ab} / s^2$ . At high values of anisotropy,  $\gamma_s \gtrsim 10^2$ , however, the shear strength is dominated by magnetic coupling between vortex segments.<sup>16,17</sup> Either by relating the critical force per vortex segment for shear slip  $f_c$  to the tilt modulus  $C_{44}$  by  $f_c \approx C_{44} a s$  and using the evaluations of the modulus for magnetic coupling,<sup>17</sup> or using directly the calculation of the shear strength,<sup>18</sup> it appears that shear slip between planes should occur for  $\partial J_{ab} / \partial z \gtrsim (c \phi_0 / 32 \pi^3 \lambda_{ab}^4) \langle \cos \varphi_{n,n+1} \rangle a / s$ . It will be seen that this condition is met with the values obtained from

the data analyzed according to the reasoning outlined below and it is a necessary condition to have a local  $\mathbf{E}(\mathbf{J})$  relation.

The above considerations lead to a scenario where the current injected and withdrawn from the same  $ab$  surface is confined by anisotropy to a penetration depth  $\sim \ell_{ab}/\gamma_s$  in the nonresistive regime with consequent enhancement of the current density. When the current density attains the critical value, for either  $J_c$  or  $J_{ab}$ , the current distribution is modified until both reach their breakdown values and the sample is resistive on one side and nonresistive on the other side of a front which advances out from each current contact point as the current is increased. As the fronts attain successive voltage contacts, these display a potential drop with respect to the portion of the sample which has remained in the nonresistive state. The shape of the resistive region can be expected to be a function of the  $\mathbf{E}-\mathbf{J}$  response around the breakdown values (vortex depinning for  $ab$  current and Josephson-junction behavior for  $c$  current) described for the most part by the anisotropy factor  $\gamma$  of the resistive state and  $\Gamma = J_{ab}^{\text{th}}/J_c^{\text{th}}$ . If the shape were determined uniquely by the  $\mathbf{E}-\mathbf{J}$  response, its position would depend only on the contact from which it originated and the magnitude of the current injected.

Restrictions are imposed on the shape of the front by the irrotational nature of the electrochemical field and by current conservation. The inductive field from the current is negligible compared to resistive fields for our pulses and sample sizes and we can suppose the field  $\mathbf{E}$  to be irrotational:  $\nabla \times \mathbf{E} = -\partial \mathbf{B}/\partial t = 0$ . We can then, as in London's treatment of breakdown in a type-I current carrying wire,<sup>1</sup> demand that  $\oint \mathbf{E} \cdot d\ell = 0$  be satisfied through the resistive/nonresistive interface (Fig. 10) with the consequence that the interface must be perpendicular to the field. As argued above, our quasipoint contact situation enforces that both  $ab$  and  $c$  breakdown appear simultaneously and the  $VI$  response in either configuration will contain both  $c$  and  $ab$  features. Either  $ab$  and  $c$  breakdown occur together at the interface or they occur alone in separated but necessarily contiguous or overlapping regions. The first case is considered in part (a) of Fig. 10 where a segment of the interface is locally oriented at an angle  $\Theta$  with the  $ab$  plane. A model with a local (locality implicitly assumes shearing of the vortex segments from plane to plane)  $\mathbf{E}-\mathbf{J}$  relation for  $\mathbf{J} > \mathbf{J}^{\text{th}}$  of the form

$$E_x = 0, \quad |J_x| \leq J_{ab}^{\text{th}}$$

$$E_x = \pm E_{ab}^{\text{th}} + \rho'_{ab}(J_x \mp J_{ab}^{\text{th}}), \quad J_x \gtrless \pm J_{ab}^{\text{th}} \quad (1)$$

$$E_z = 0, \quad |J_z| \leq J_c^{\text{th}}$$

$$E_z = \pm E_c^{\text{th}} + \rho'_c(J_z \mp J_c^{\text{th}}), \quad J_z \gtrless \pm J_c^{\text{th}} \quad (2)$$

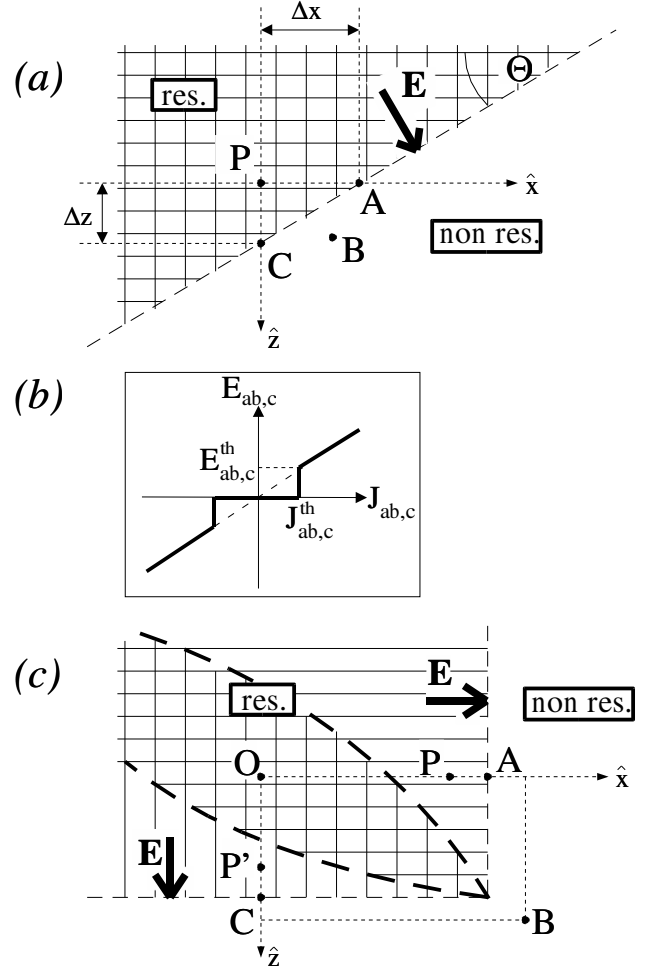


FIG. 10: The upper part (a) of the figure illustrates the condition that the electric field be perpendicular to any segment of the resistive/nonresistive interface supposing spatially coincident  $ab$  and  $c$  current breakdown; “res” denotes the resistive side, “nonres” the nonresistive side.  $E_{ab}$  and  $E_c$  are given by the  $\mathbf{E}(\mathbf{J})$  relationship, an example of which is shown in part (b). Positive differential resistivities for both components imply both  $\partial J_{ab}/\partial x_{ab} > 0$  and  $\partial J_c/\partial x_c > 0$ , in contradiction with current conservation which requires that these two derivatives have opposite signs (for a 2D distribution). If however one of the two current-density components is subcritical,  $\Theta = 0, \pi/2$ , the corresponding derivative is free. The latter situation is illustrated in the lower part of the figure where in addition the front changes orientation from  $\Theta = 0$  to  $\Theta = \pi/2$  within the sample, a situation which is still compatible with the irrotationality condition  $\oint \mathbf{E} \cdot d\ell = 0$  on the electric field provided that the resistive region between pure  $ab$  and pure  $c$  breakdown also terminates at the corner of the rectangle.

on the resistive side is shown in part (b) of the figure.  $\rho'_{ab}$  and  $\rho'_c$  are the dynamic resistivities in the  $ab$  and  $c$  direction in the superconductive state beyond breakdown. The condition that the field be perpendicular to the interface would demand that  $\tan \Theta = \Delta z/\Delta x = \pm E_{ab}^{\text{th}}/E_c^{\text{th}}$ , where the  $E_{ab}^{\text{th}}$  and  $E_c^{\text{th}}$  components of the electrochemical

field both point towards the interface, in the directions of the  $ab$  and  $c$  components of the current flow. However because both components of the current density must diminish on approaching the interface,  $\partial J_x/\partial x$  and  $\partial J_y/\partial y$  both have the same sign whereas current conservation  $\nabla \cdot \mathbf{J} = 0$  requires them to have opposite signs. More explicitly, if the interface is imagined to have positive intercepts with the axes of an  $(\hat{x}, \hat{z})$  coordinate system whose origin is at  $P$  in the resistive region as in Fig. 10, both  $J_x > J_{ab}^{\text{th}}$  and  $J_z > J_c^{\text{th}}$  (all with positive values, current flowing from left to right and top to bottom). But the fact that the current diminishes on approaching the interface along each of the principal directions to reach  $J_{ab}^{\text{th}}$  and  $J_c^{\text{th}}$  which defines the interface imposes that both  $\partial J_x/\partial x < 0$  and  $\partial J_z/\partial z < 0$  at the same point  $P$ , in violation of current conservation which demands that  $\partial J_x/\partial x = -\partial J_z/\partial z$ .

We conclude that a region of spatially coincident  $ab$  and  $c$  breakdown may not have an interface with the nonresistive region.

Resistive/nonresistive interfaces perpendicular to pure  $ab$  or pure  $c$  breakdown, however, do not violate current conservation. For sole  $c$  breakdown,  $J_z > J_c^{\text{th}}$ ,  $J_x < J_{ab}^{\text{th}}$  at the interface and the positive  $\partial J_x/\partial x$  which must result from the negative  $\partial J_z/\partial z$  to conserve current has no consequence for the electric field because the  $x$  component is subcritical and produces no electric field. A similar argument can be made for pure  $ab$  breakdown, establishing that nonresistive/resistive interfaces are possible for single-component breakdown whereas they are not for spatially coincident two-component breakdown. Furthermore it is possible to change the orientation of the interface between the two perpendicular principal directions of the superconductor on the condition that the two separated mutually perpendicular  $ab$  and  $c$  fronts meet at a common point and that the interface between the two types of breakdown converges to the same point. The latter interface could be either a simple common boundary or more generally a lens shaped region of coincident  $ab$  and  $c$  breakdown. Such a situation is illustrated in part (c) of Fig. 10. We conclude that the fronts must be formed of segments of interfaces perpendicular to pure  $ab$  or pure  $c$  current breakdown. Numerical solutions of the model<sup>19</sup> indicate a simple rectangle with a generic form of the type illustrated in Fig. 11.

The length  $\ell$  and depth  $d$  of the resistive region are related to the current by

$$I = w(dJ_{ab}^{\text{th}} + \ell J_c^{\text{th}}), \quad (3)$$

where  $w$  is the width of the sample. The threshold current measured for the potential between the nonresistive region and a contact on the surface at a distance  $\ell_1$  from the current injection contact is given by the condition that the front arrives at the contact,  $\ell = \ell_1$ :

$$I_{\ell_1}^{\text{th}} = w\ell_1(J_{ab}^{\text{th}}d/\ell + J_c^{\text{th}})$$

and for a voltage contact at depth  $d_1$  by  $d = d_1$ :

$$I_{d_1}^{\text{th}} = wd_1(\ell/d)(J_{ab}^{\text{th}}d/\ell + J_c^{\text{th}}),$$

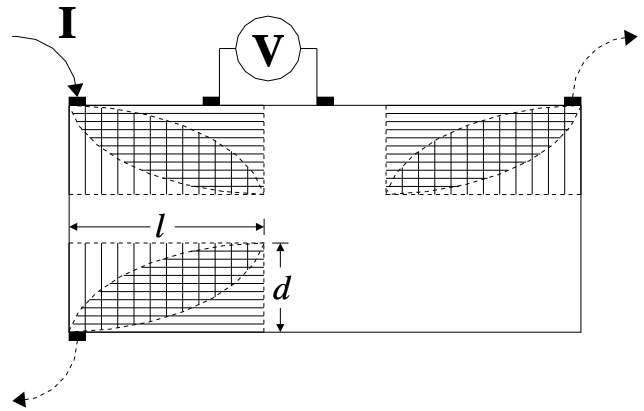


FIG. 11: Generic form of resistive regions. The dotted current withdrawal arrows are  $ab$  and  $c$  configuration alternatives. Horizontal lines indicate  $ab$  breakdown, vertical lines  $c$  breakdown.

provided that  $\ell(I)$  is sufficient that the front attains the contact in the  $\hat{x}$  direction ( $I_{\ell_1}^{\text{th}} > I_{d_1}^{\text{th}}$ ). In general,  $\ell = \ell(I)$  and  $d = d(I)$ , but if there are no other relevant lengths in the problem (distances between  $ab$  configuration current contacts  $\ell_{ab} \gg \ell$  and  $c$  configuration current contacts  $\ell_c = t \gg d$ ) one can expect the ratio  $\ell/d$  to be independent of the current and only a function of the anisotropy factors  $\gamma$  and  $\Gamma = J_{ab}^{\text{th}}/J_c^{\text{th}}$ . If we interpret the top and terrace thresholds of the experiment on sample  $C$  as measurements of  $I_{\ell_1}^{\text{th}}$  and  $I_{d_1}^{\text{th}}$  and we make the hypothesis that the aspect ratio  $\ell/d$  is independent of current, then the measurements tell us that

$$\ell/d = (\ell_1/d_1)(I_{d_1}^{\text{th}}/I_{\ell_1}^{\text{th}}) \approx 2500$$

and

$$J_{ab}^{\text{th}}d/\ell + J_c^{\text{th}} \approx 10 \text{ A cm}^{-2} \quad (4)$$

or, multiplying by  $\ell/d$ ,

$$J_{ab}^{\text{th}} + J_c^{\text{th}}\ell/d \approx 2.5 \times 10^4 \text{ A cm}^{-2}, \quad (5)$$

where the last two quantities are the same combination of  $ab$  and  $c$  transport properties which we cannot separate without a model calculation for the aspect ratio of the resistive front. This will be the subject of a future paper<sup>19</sup> on numerical solutions of the present model.

The upper limits on  $J_c^{\text{th}}$  and  $J_{ab}^{\text{th}}$  given by relations (4) and (5) are consistent with the value  $J_c^{\text{th}} \approx 2 \text{ A cm}^{-2}$  obtained from combining  $J_J$  measured in the mesa experiment with  $\langle \cos \varphi_{n,n+1} \rangle \approx 4 \times 10^{-3}$  extrapolated from the Josephson plasma resonance experiments<sup>13</sup> and the value  $J_{ab}^{\text{th}} \approx 2 \times 10^4 \text{ A cm}^{-2}$  estimated from the magnetic hysteresis.<sup>15</sup> The condition for slip between planes is well satisfied for these values indicating that the description is self-consistent.



## VI. SUMMARY

The experimental results on  $VI$  characteristics for  $ab$  surface contacted samples of the highly anisotropic BSCCO superconductor in the low-temperature vortex lattice phase above about 2000 Oe show that the  $VI$  responses for  $ab$  or  $c$  current configurations are virtually identical and that the dissipative region invades the samples in the form of a resistive/nonresistive front moving out from the current contacts with increasing current. The  $VI$  characteristic depends only on current magnitude, voltage contact position and nearest current injection point. It is argued that current penetration in the nonresistive regime is limited by the high anisotropy to depths less than the London screening length, and that the resistive region must involve simultaneous  $ab$  and  $c$  breakdown and shear of successive planes of vortex segments. The shape of the resistive region is argued to be composed of rectangular segments and seems to be a simple rectangle with interfaces to the nonresistive portion consisting of pure  $ab$  or pure  $c$  breakdown. A different contact arrangement using an ion etched terrace to

sample the potential in the depth of the sample brings extra information that allows access to the aspect ratio of the rectangle. But because the  $ab$  and  $c$  configuration experiments measure the same combination of  $ab$  and  $c$  properties, it is necessary to propose and solve a specific model to separate them. A detailed discussion of numerical solutions of the model has been reserved for future publication.

## Acknowledgments

We take pleasure in acknowledging discussion with I. Tüttő and L. F. Kiss. We are grateful to L. Forró and to B. Keszei for supplying the crystals used in this study. B.S. and Á.P. acknowledge the Atomic Energy Commission for a Bursary to visit the Saclay laboratory. Research in Hungary has been supported by Grant Nos. OTKA T037976 and TS040878. We are grateful also for the support of the “BALATON” Collaboration program of the French and Hungarian Foreign Affairs Ministries.

- 
- <sup>1</sup> F. London, *Superfluids*, vol. I (Dover, New York, 1960).
- <sup>2</sup> W. E. Lawrence and S. Doniach, in *Proceedings of the XIIth International Conference on Low Temperature Physics*, edited by E. Kanda (Keigaku, Tokyo, 1971), p. 361.
- <sup>3</sup> R. Busch, G. Ries, H. Werthner, G. Kreiselmeyer, and G. Saemann-Ischenko, *Phys. Rev. Lett.* **69**, 522 (1992).
- <sup>4</sup> D. T. Fuchs, E. Zeldov, M. Rappaport, T. Tamegai, S. Ooi, and H. Shtrikman, *Nature (London)* **391**, 373 (1998).
- <sup>5</sup> B. Sas, F. Portier, K. Vad, B. Keszei, L. F. Kiss, N. Hegman, I. Puha, S. Mészáros, and F. I. B. Williams, *Phys. Rev. B* **61**, 9118 (2000).
- <sup>6</sup> E. Rodríguez, M. F. Goffman, A. Arribére, F. de la Cruz, and L. F. Schneemeyer, *Phys. Rev. Lett.* **71**, 3375 (1993).
- <sup>7</sup> B. Keszei, G. Szabó, J. Vandlik, L. Pogány, and G. Oszlányi, *J. Less Common Met.* **155**, 229 (1989).
- <sup>8</sup> J. R. Cooper, L. Forró, and B. Keszei, *Nature (London)* **343**, 444 (1990).
- <sup>9</sup> F. Portier, G. Kriza, B. Sas, L. F. Kiss, I. Pethes, K. Vad, B. Keszei, and F. I. B. Williams, *Phys. Rev. B* **66**, 140511 (2002).
- <sup>10</sup> L. N. Latyshev and T. Yamashita, *Phys. Rev. Lett.* **82**, 5345 (1999).
- <sup>11</sup> V. Ambegaokar and A. Baratoff, *Phys. Rev. Lett.* **10**, 486 (1963).
- <sup>12</sup> Y. Matsuda, M. B. Gaifullin, K. Kumagai, K. Kadowaki, and T. Mochiku, *Phys. Rev. Lett.* **75**, 4512 (1995).
- <sup>13</sup> T. Shibauchi, T. Nakano, M. Sato, T. Kisu, N. Kameda, N. Okuda, S. Ooi, and T. Tamegai, *Phys. Rev. Lett.* **83**, 1010 (1999).
- <sup>14</sup> M. B. Gaifullin, Y. Matsuda, N. Chikumoto, J. Shimoyama, and K. Kishio, *Phys. Rev. Lett.* **84**, 2945 (2000).
- <sup>15</sup> B. Khaykovich, D. T. Fuchs, K. Teitelbaum, Y. Myasodov, E. Zeldov, T. Tamegai, S. Ooi, M. Konczykowski, R. A. Doyle, and S. F. W. R. Rycroft, *Phys. Rev. B* **61**, R9261 (2000).
- <sup>16</sup> A. Buzdin and D. Feinberg, *J. Phys. (France)* **51**, 1971 (1990).
- <sup>17</sup> A. E. Koshelev and P. H. Kes, *Phys. Rev. B* **48**, 6539 (1993).
- <sup>18</sup> T. Pe, M. Benkraouda, and J. R. Clem, *Phys. Rev. B* **55**, 6636 (1997).
- <sup>19</sup> G. Kriza *et al.* (unpublished).
- <sup>20</sup> Fuchs and collaborators (Ref. 4) have done a very interesting experiment to determine the distribution of the  $\hat{c}$ -directed component of the current-induced magnetic field across and just outside a current carrying sample. In the low-temperature phase which interests us here, they deduce that there is a stronger current density on the edge of the sample. Their observations are compatible with the expected finite width correction  $j_x = [1 - (2y/w)^2]^{-1/2}$ , where  $w$  represents the full width and  $y$  is measured from the midline. This distribution is constructed to ensure the zero  $\hat{c}$ -directed induced field in the sample as required by the superconducting state with fixed vortices.